NANO LETTERS

pubs.acs.org/NanoLett Letter

Electronic Exciton–Plasmon Coupling in a Nanocavity Beyond the Electromagnetic Interaction Picture

Antton Babaze,* Ruben Esteban, Andrei G. Borisov, and Javier Aizpurua*

Cite This: *Nano Lett.* 2021, 21, 8466–8473 Read Online

ACCESS | Metrics & More | Article Recommendations | Supporting Information

ABSTRACT: The optical response of a system formed by a quantum emitter and a plasmonic gap nanoantenna is theoretically addressed within the frameworks of classical electrodynamics and the time-dependent density functional theory (TDDFT). A fully quantum many-body description of the electron dynamics within TDDFT allows for analyzing the effect of electronic coupling between the emitter and the nanoantenna, usually ignored in classical descriptions of the optical response. We show that the hybridization between the electronic states of the quantum emitter and those of the metallic nanoparticles strongly modifies the energy, the width, and the very existence of the optical resonances of the coupled system. We thus conclude that the application of a quantum many-body treatment that correctly addresses charge-transfer processes between the emitter and the nanoantenna is crucial to address complex electronic processes involving plasmon–exciton interactions directly impacting optoelectronic applications.

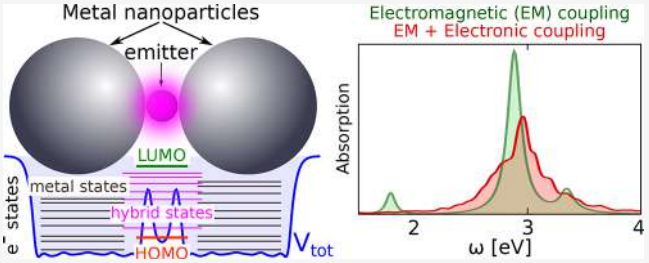

KEYWORDS: *plasmonics, time-dependent density functional theory, quantum emitter, electromagnetic coupling, charge transfer, optoelectronic response, optical nanoantenna, strong coupling*

A quantum emitter (QE), such as an organic molecule or a quantum dot, placed in the vicinity of metal nanoparticles (MNPs), represents a system of paramount importance in a variety of spectroscopy and microscopy techniques in nanophotonics, such as in surface-enhanced fluorescence,[1−3] single-molecule microscopy,[4,5] and lifetime correlation spectroscopy,[6] among others. The main mechanism that controls the optical interaction and light emission in these hybrid systems is the energy transfer between localized surface plasmons in the MNPs and the excitons formed in the QE. Intense experimental and theoretical efforts have been devoted to study the role of plasmon–exciton coupling to modify the energy and the spontaneous emission rate of a QE, as well as to create a new type of exciton–plasmon polaritonic states that drastically change the optical absorption and emission spectral fingerprints.[7−13]

In this context, diverse theoretical approaches have been adopted to tackle optical excitations in QE–MNP hybrid systems, including classical descriptions[14−20] with a parametric account for the nonlocality of the metal response,[21−26] as well as cavity quantum electrodynamics (c-QED) descriptions that naturally address the dynamics of the polaritonic states involved.[27−30] Moreover, other models that combine a quantum-chemistry description of the QE atomistic structure with a classical electrodynamics approach of the optical QE–MNP interaction[31−33] have also been employed to address complex experimental situations as, for instance, in hyper-resolved fluorescence microscopy with subnanometric resolution.[4,5,34,35]

The success of the aforementioned methodologies to explain the main features of light emission in plasmonic nanocavities is due to the dominance of the electromagnetic interaction in the QE–MNP coupling for separations as small as one nanometer.[14,36] However, at smaller separations between emitters and metal surfaces, of the order of Ångstroms, another quantum effect becomes important: electronic states localized at the QE and at the MNP hybridize into "supermolecular" states which modify optical transitions, allowing for electron transfer between the QE and the MNP.

Despite its importance,[36−40] the effect of the hybridization between the QE and the MNP electronic states as well as the corresponding electron-transfer processes remain largely unexplored in nanophotonics, as the quantum theoretical treatment of the problem is challenging. It is only recently that such studies have become within the reach of theoretical efforts,[41−45] enabling a better understanding of light emission in tunneling junctions.[46−49] Notably, it has been shown that a QE bridging metallic nanoparticles can trigger electron conductance across subnanometric junctions, which strongly influences the optoelectronic response.[41−44,50]

Received: August 18, 2021
Published: September 16, 2021

https://doi.org/10.1021/acs.nanolett.1c03202
Nano Lett. 2021, 21, 8466–8473

In this work, we apply a quantum many-body approach to study the optical response and exciton dynamics in a QE−MNPs system where the emitter is located at subnanometric separation from the metallic interfaces. We place particular emphasis on the role of electronic coupling and electron transfer between the QE and the MNP to unveil the manifestation of these quantum effects in the optical response of the entire coupled system. Importantly, we demonstrate that the modification of the electronic structure of the hybrid system as well as the broadening of the electronic states of the QE due to charge transfer lead to a breakdown of the classical electromagnetic description of the plasmon−exciton interaction. We reveal important quantitative and qualitative differences between quantum and classical results of the line widths and energies of the relevant optical modes. Moreover, we also observe the formation of a new charge-transfer plasmon mode at low energies mediated by the emitter electronic structure.

As a model system, we consider a QE interacting with a plasmonic dimer antenna formed by two spherical MNPs, which is a canonical configuration thoroughly analyzed in the literature using classical approaches.[15,51−54] As sketched in Figure 1a, the QE placed in the middle of a plasmonic nanogap is illuminated by a plane wave polarized along the dimer axis (z-axis). Within our study, the gap separation D is varied to explore different regimes of electronic QE−MNPs coupling, ranging from electronically decoupled QE−MNPs (large D) to electronically coupled ones (small D). The calculation of the optical response is performed within the Kohn−Sham scheme of time-dependent density functional theory[55−58] (TDDFT), which successfully incorporates quantum phenomena such as many-body and electron−hole pair excitations, electronic spill-out, nonlocal screening, or electron tunneling in (sub)-nanometric metallic cavities.[59−67] Because of the small size of the system, retardation effects are neglected in the present work. Atomic units (au) are used throughout this manuscript unless otherwise stated.

The electronic structure of the MNPs is described within the jellium model of free-electron metals,[68,69] which correctly predicts the main quantum effects in plasmonics as confirmed by experimental studies and by comparison with atomistic *ab initio* calculations.[64,70] The electron density is defined by a Wigner−Seitz radius of $r_s = 4$ a_0, which corresponds to sodium ($a_0 = 0.053$ nm is the Bohr radius). This particular density parameter is chosen here because, for this value, the jellium nanoparticle plasmons fall within the typical optical frequency range. Each MNP contains 638 conduction electrons (radius $R_{MNP} = 34.4$ $a_0 \approx 1.8$ nm), and the Fermi level of the MNPs stands at $E_F = -2.86$ eV below the vacuum level. We also adopt the jellium model to describe the QE as a spherical object of radius $R_{qe} = 5$ a_0 (≈0.26 nm) containing two (spin-degenerated) electrons. The model QE represents a two-level system with a 1s ($m = 0$, with m the magnetic quantum number) highest occupied molecular orbital (HOMO), and a triply degenerate 2p ($m = 0, \pm 1$) lowest unoccupied molecular orbital (LUMO). Thus, the optical absorption of the QE is determined by the 1s → 2p transition. The potential profile of the QE−MNPs system and the corresponding ground-state electron density are shown in Figure 1b,c, respectively, for a gap separation of $D = 26$ a_0. As we discuss below, our main findings are robust with respect to the model description of the QE and MNPs. In the Supporting Information, we provide further details on the calculation of the electronic structure of the QE and MNPs as well as on the current implementation of the Kohn−Sham scheme of TDDFT, also reported in ref 59.

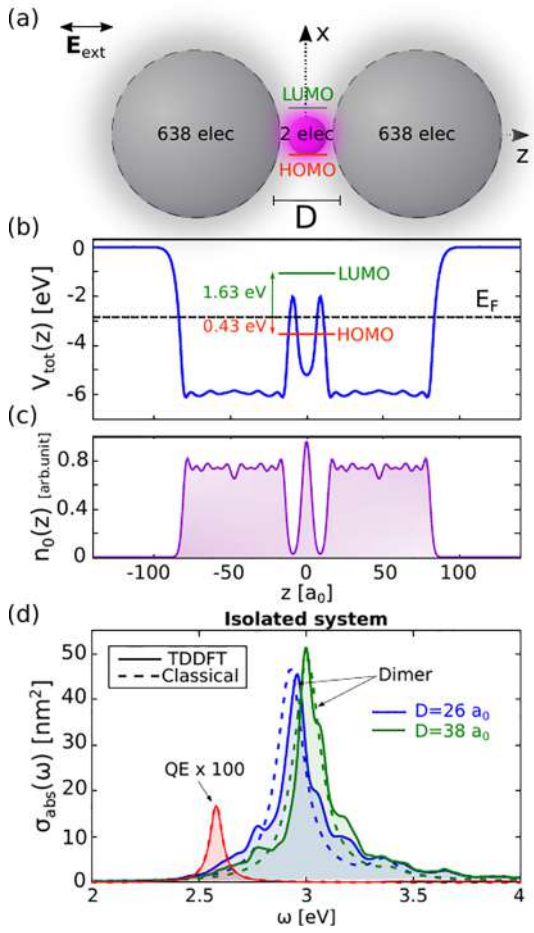

Figure 1. (a) Sketch of the system under study. A quantum emitter with a single optically allowed HOMO−LUMO transition is located in the middle of the gap of size D formed by two spherical metallic nanoparticles (MNPs). The quantum emitter and each metallic nanoparticle contain 2 and 638 conduction electrons, respectively. (b) Total one-electron potential $V_{tot}(\mathbf{r})$ and (c) ground-state electron density $n_0(\mathbf{r})$ along the symmetry z-axis for the coupled QE−MNPs system with gap size $D = 26$ a_0. The HOMO ($E_{homo} = -3.29$ eV) and LUMO ($E_{lumo} = -1.23$ eV) energy levels of the isolated QE are represented by red and green lines, respectively. The Fermi level $E_F = -2.86$ eV of the MNPs is shown by the black dashed line. (d) Absorption spectra of the isolated metallic dimer for $D = 26$ a_0 (blue line) and $D = 38$ a_0 (green) and of the isolated quantum emitter (red line). Dashed and solid lines correspond to the results obtained with classical and TDDFT simulations, respectively.

Prior to studying the coupled QE−MNPs system, it is useful to analyze the optical response of the uncoupled constituents. In Figure 1d, we show the absorption spectra of an isolated metallic dimer characterized by gap sizes of $D = 38$ a_0 and $D = 26$ a_0, as well as that of the isolated QE, as calculated within TDDFT (solid lines). The optical response of the dimer is characterized by a bonding dipolar plasmon (BDP) resonance at $\omega_{BDP} \sim 3$ eV. As expected, this BDP mode redshifts when reducing the gap separation because of the increased capacitive coupling between the two MNPs.[71] We first consider the exciton energy ω_0 of the isolated QE to be $\omega_0 = 2.58$ eV, with the absorption cross section more than 2 orders of magnitude weaker than that of the nanoantenna BDP. As a reference, in Figure 1d, we also show the results from classical local

https://doi.org/10.1021/acs.nanolett.1c03202
Nano Lett. 2021, 21, 8466−8473

calculations (dashed lines). Here, the QE is described as a point-like dipole[14,16] with an oscillator strength α_0 = 1.7 au, a resonant energy ω_0 = 2.58 eV and a decay rate γ_{qd} = 70 meV. The MNPs are described using a Drude dielectric function parametrized according to the absorption spectrum of the individual MNP calculated with TDDFT,[59] and the gap size is scaled in order to account for the dynamical screening.[72] Thus, nonlocal effects are partially introduced in the classical calculations, which allows us to correctly reproduce the absorption spectra as calculated with TDDFT for the isolated constituents (see Supporting Information for further details).

Once the optical response of the isolated constituents has been determined, one can analyze the quantum effects emerging in the optical response of the hybrid system due to the optoelectronic QE−MNPs coupling. To this end, we compare classical and quantum TDDFT results of the absorption cross section of the QE−MNPs system as a function of gap separation D, as shown in Figure 2a,b with waterfall plots. The gap separation is varied from D = 40 a_0 to D = 16 a_0, which allows for covering different interaction regimes and for observing the onset of electronic hybridization in the system.

To make an intuitive link with the classical picture of the point-dipole emitter in proximity to a plasmonic nanoantenna, we first outline the classical results of the absorption spectra shown in Figure 2a. Three resonant features are obtained within the framework of classical electromagnetic theory: a lower resonance (LR; blue dots) shifting from $\omega_{LR} \sim 2.5$ eV to ~1.8 eV as the gap separation is reduced, an upper resonance (UR; green dots) at $\omega_{UR} \sim 3$ eV, and a bonding quadrupolar plasmon (BQP; red dots) at $\omega_{BQP} \sim 3.4$ eV, more pronounced for narrow gaps.

For large interparticle distances, D = 30−40 a_0, the spectra of Figure 2b obtained within the TDDFT approach are in good agreement with classical results (Figure 2a). Indeed, in this situation, the electron densities of the individual nanoconstituents do not spatially overlap, as there is negligible hybridization between their electronic orbitals. At these large separations, the assignment of the underlying modes can be performed using their asymptotic behavior. First, the LR can be associated with the QE exciton. This excitonic energy is slightly redshifted with respect to the transition energy of the isolated QE due to the interaction with the MNPs (Lamb shift).[73] The TDDFT calculations of the induced electron density confirm the excitonic nature of the LR branch, characterized by a strongly polarized QE, as observed in the top-left panel of Figure 2c. On the other hand, the UR at $\omega_{UR} \sim 3$ eV is associated with the BDP plasmon mode of the isolated metallic dimer. The induced electron density at the QE appears polarized in the direction opposite to the main dipole induced at the MNPs, since ω_{UR} is higher than the QE exciton energy ω_0 (see right panels of Figure 2c).

Upon decreasing the gap separation (interparticle distance below D = 26 $a_0 \approx$ 1.4 nm), the quantum nature of the electron dynamics strongly affects the overall shape of the absorption profile. The BQP mode shown by the classical approach at $\omega_{BQP} \sim 3.4$ eV is not developed in the TDDFT results. This is because, for these small particles, the diffuse nature of the electron density at the nanoparticle surface captured by the quantum TDDFT framework prevents the formation of high-order plasmonic resonances.[26,74,75] Moreover, for small gap separations, the TDDFT simulations predict a smaller redshift and stronger broadening of the UR

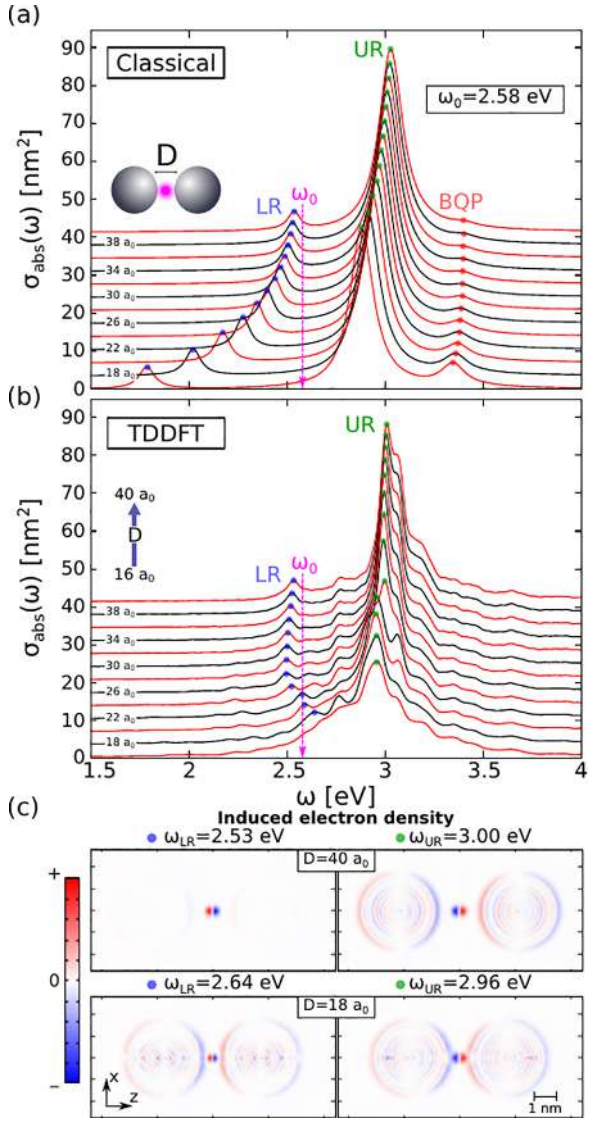

Figure 2. Optical absorption of the hybrid QE−MNPs system. (a, b) Waterfall plot of the absorption spectra as obtained from (a) classical and (b) TDDFT simulations for a gap size ranging from D = 16 a_0 to D = 40 a_0 in steps of 2 a_0. The D value is indicated at each second spectra marked by the black line. Results are shown as a function of frequency, ω. The transition frequency ω_0 = 2.58 eV of the isolated QE is marked with a vertical magenta arrow in both panels. The blue (LR), green (UR), and red (BQP) dots indicate the resonance frequencies of the main modes of the system. (c) TDDFT results of the induced electron density at the LR (left-side panels) and UR (right-side panels) resonances (red for positive and blue for negative sign). The resonance frequency is indicated at the top of each panel. Upper panels correspond to a gap size D = 40 a_0, and lower panels to D = 18 a_0, as indicated. Each snapshot is taken at the instant of time t when the total dipole moment of the system is maximum. Results are plotted in the (x,z)-plane, and the system holds axial symmetry with respect to the z-axis.

branch as compared to classical results. These effects can be mainly ascribed to quantum phenomena such as nonlocality and finite-size effects that are important for such small MNPs, but also to electron transport between the MNPs mediated by the electronic structure of the QE,[44] as we further confirm in the Supporting Information. The induced electron density shown in the bottom-right panel of Figure 2c indicates that the

https://doi.org/10.1021/acs.nanolett.1c03202
Nano Lett. 2021, 21, 8466−8473

BDP character of the UR mode is preserved for these small separations.

The most dramatic difference between quantum and classical results is observed for the LR branch with excitonic asymptotic character. Classical calculations predict a strong and continuous redshift of the LR with a decreasing gap size due to the electromagnetic interaction, i.e., the interaction between the QE exciton dipole and its induced screening charges at the surfaces of the MNPs across the gap. In sheer contrast with this classical prediction, within the quantum model, the LR branch blueshifts with a decreasing gap size for $D \leq 26$ a_0 and gradually disappears, losing its excitonic character and evolving into a broad low-frequency shoulder of the UR for the smallest gap size considered in Figure 2b (D = 16 a_0). This can be observed in the bottom-left panel of Figure 2c, where the loss of the exciton character can be identified through the spread of the induced electron density over the MNPs (compare to the top-left panel).

The blueshift of the LR branch with decreasing separation and its subsequent disappearance are direct consequences of the hybridization between the electronic states of the QE and those of the MNPs. The excited electron initially localized on the 2p LUMO of the QE can tunnel through the potential barrier that separates the QE from the MNPs. The electron transfer from the QE into the empty states of the MNPs above the Fermi level results in the quenching of the QE signature in the optical response.[40] This electronic interaction between the QE and the MNPs can be clearly observed in Figure 3, where

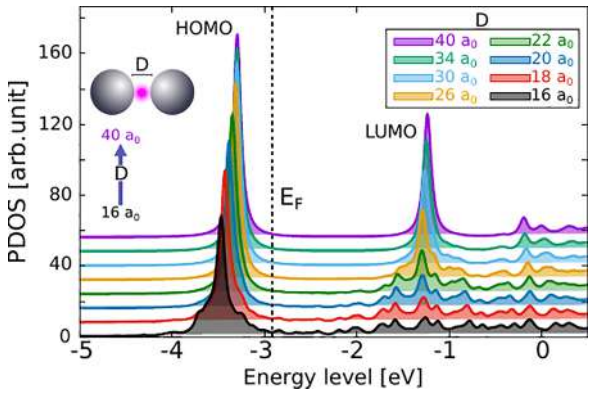

Figure 3. Projected density of electronic states (with m = 0 symmetry) localized at the QE in the middle of the gap. Here m is the projection of the electron angular momentum on the quantization z-axis. Results are shown as a function of the electron energy for different values of the gap size D ranging from D = 16 a_0 to D = 40 a_0 as displayed in the inset. The Fermi level E_F = −2.86 eV of the MNPs is depicted by a vertical dashed line.

we show the evolution of the projected density of electronic states (PDOS),[76] upon decreasing the dimer gap separation D. Due to the azimuthal symmetry of the system, the magnetic quantum number m is a preserved quantity so that the HOMO state can only couple to electronic states with m = 0. Consistently, the PDOS is calculated within the m = 0 symmetry subspace in the region of the QE. Details on the PDOS calculations can be found in the Supporting Information.

For a large separation distance, $D \sim 30$−40 a_0, the PDOS shows two well-defined peaks corresponding to the HOMO and LUMO of the individual QE. Thus, the excitation of the HOMO−LUMO 1s → 2p electronic transition leads to an induced dipole moment that can be correctly described within a classical point-dipole approximation. However, upon reducing D, the states localized at the QE experience a broadening, which reveals an increase in the rate of electron transfer between the QE and the MNPs.[76] The HOMO has higher binding energy, and thus, it is more localized in space as compared to the LUMO. For this reason, the coupling of the HOMO with the metal nanoparticles is smaller, and its resonance in the PDOS is well defined and preserved even for the smallest separation of the gap, D = 16 a_0, considered here. As D is decreased, the HOMO energy shifts to lower values, owing to the increase of the Coulomb interaction with the MNPs. In contrast, the less bound and thus more spatially extended LUMO strongly hybridizes with the unoccupied states of the MNPs. As a consequence, the LUMO resonance in the PDOS dramatically broadens when narrowing the gap. For gaps smaller than $D \sim 20$ a_0, the peak of the LUMO state vanishes, revealing the absence of a well-defined unoccupied electronic state localized in the QE that could be optically accessible. We can describe this effect as the quenching of the QE-localized dipole expressed in the optical excitation.[40] Indeed, in this situation, the excited electron is shared between the QE LUMO and the MNPs states.

The modifications of the HOMO and LUMO by the electronic interactions between the QE and the MNPs shown in Figure 3 drastically affect the coupling between the QE excitation and light as identified in Figure 2b and lead to (i) blueshift of the LR mode for gap sizes below $D \sim 26$ a_0 and (ii) progressive transformation of the LR mode into a broad spectral feature appearing as a shoulder of the UR mode. The excitation, in this case, is built up by the hole localized in the HOMO of the QE and an excited electron delocalized over the QE−MNPs system.

We next discuss in Figure 4 the role of the QE in triggering electron transport between the two nanoparticles across the junction in response to external illumination. In the last years, several works have identified the emergence of charge-transfer plasmons (CTP) supported in metallic vacuum junctions for gap separations typically below ∼0.4 nm and resonant frequencies of the order of a few electronvolts.[65,70,77−83] Moreover, as pointed out in previous works,[41−44,50] the presence of a QE bridging a metallic nanogap substantially modifies the charge-transfer properties of the system and triggers out the emergence of low-energy resonances associated with electron transport between the nanoparticles.

As discussed above (Figure 3), for narrow junctions, the spectral weight of the LUMO is distributed over the electronic states of both MNPs, allowing for electron tunneling between the MNPs through the QE.[44] Moreover, for gap separations of $D \sim 18$ a_0 and below, the QE gives rise to a depletion of the potential barrier close to the dimer axis below the Fermi level of the system (Figure 4a) so that even a classically allowed over-the-barrier electron transport between the MNPs becomes possible. As a consequence, for gap sizes D = 12 a_0 − 18 a_0 ($D \approx 0.6$−0.95 nm, thus larger than typical tunneling distances in metal−vacuum−metal junctions), a charge-transfer resonance emerges in the low-energy region of the absorption spectra, $\omega_{CT} \sim 0.1$−0.2 eV (Figure 4b), consistent with results reported in the literature.[41,42,50] This new resonance is only activated due to the presence of the QE (see the response of the isolated dimer depicted by the dashed line), and it blueshifts and strengthens considerably when

https://doi.org/10.1021/acs.nanolett.1c03202
Nano Lett. 2021, 21, 8466−8473

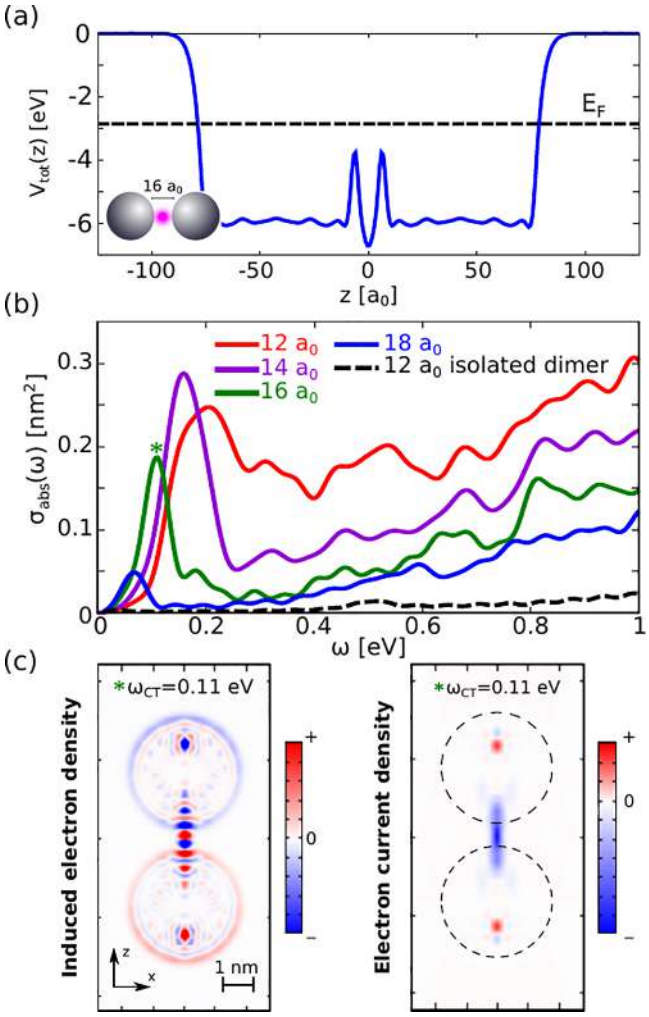

Figure 4. (a) Ground-state potential V_{tot} along the symmetry z-axis of the hybrid QE−MNPs system for D = 16 a_0. (b) Absorption spectra of the hybrid QE−MNPs system for low illumination frequencies ω = 0−1 eV. Results are shown for a gap size D ranging from D = 12 a_0 to D = 18 a_0, as indicated in the inset. The reference absorption spectrum of the isolated metallic dimer for D = 12 a_0 is shown by the dashed black line. (c) Color maps of the induced electron density (left) and the electron-current density along the z-direction (right) for an incident z-polarized electromagnetic plane wave of frequency ω_{CT} = 0.11 eV. The gap distance is D = 16 a_0. In the right-side panel, the boundaries of the jellium edges of the MNPs are indicated by dashed lines. The snapshots are taken at the instants of time when the total dipole moment (left-side panel) and the electron-current density at the middle of the junction (right-side panel) are maximum.

decreasing the interparticle distance. The charge-transfer character of the mode is clearly revealed by the induced electron density shown in Figure 4c (left-side panel), with each MNP exhibiting a monopolar density pattern of opposite sign, and it is further corroborated by the electron-current density along the z-direction[83] (right-side panel), which clearly shows that electrons shuttle from one nanoparticle to another. Similar results are obtained for other QE configurations with different HOMO and LUMO energy levels (see Supporting Information). Thus, the low-energy charge-transfer plasmon reported here can be understood as a consequence of the ballistic electron transport and does not require the tunneling mechanism aid by a localized state at the QE.[43]

Finally, we show that the effect of the delocalization of the QE excited electron on the optical response of the system is a general and robust effect. This delocalization is derived from the electronic coupling between the QE and the MNPs regardless of the electromagnetic coupling regime. Figure 5

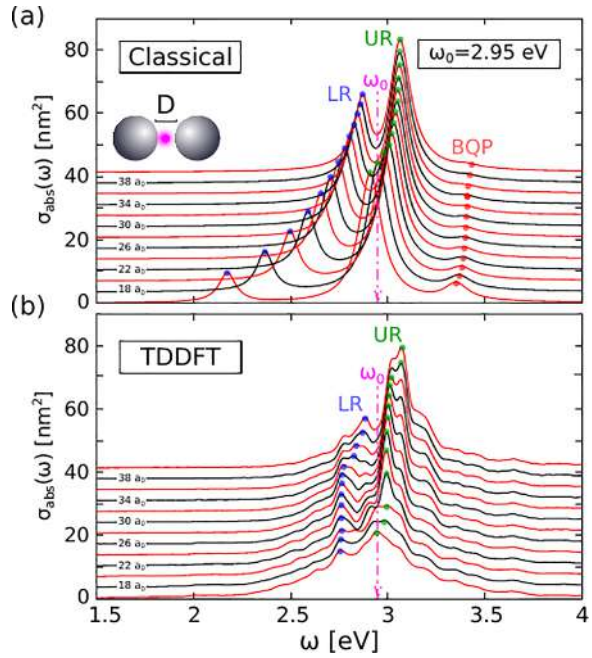

Figure 5. Waterfall plots of the optical absorption spectra of a resonantly coupled QE−MNPs system. The incident electromagnetic plane wave is polarized along the dimer axis (z-axis). The exciton energy of the isolated QE, ω_0 = 2.95 eV (marked with vertical magenta arrows), is close to the BDP resonance of the metallic dimer. The (a) classical and (b) TDDFT results are shown as a function of the frequency ω for gap sizes ranging from D = 16 a_0 to D = 40 a_0 in steps of 2 a_0. To obtain the classical results, the parameters of the local Drude dielectric function are adjusted to recover the TDDFT results, and the gap separation is scaled, so that nonlocal effects are effectively included. The D value is indicated at each second spectra marked by the black lines. The blue (lower resonance, LR), green (upper resonance, UR), and red (bonding quadrupolar plasmon, BQP) dots indicate the main modes of the system.

shows the absorption spectra obtained for a QE exciton energy ω_0 = 2.95 eV resonant with the BDP of the nanoantenna, as calculated from classical (panel a) and TDDFT (panel b) simulations. Differently to the previous case shown in Figure 2 (weakly coupled QE−MNPs due to detuning), in this situation, the system would be classically in the strong-coupling regime[25,45,84] (Figure 5a), with the UR−LR splitting considerably increasing upon reduction of the gap size D (see section S4 of Supporting Information for detailed discussion). Despite this very different electromagnetic coupling regime, the TDDFT results (Figure 5b) reveal very similar trends to those found for the off-resonant case in Figure 2. Indeed, the electronic hybridization in this strongly coupled system hinders the energy transfer between the QE and the MNPs, thus attenuating the UR-LR splitting in exciton−plasmon polariton systems as well as producing a progressive merging of the LR and UR branches into a broad spectral feature when decreasing gap separation D. In this situation, strong electromagnetic coupling is, therefore, frustrated due to electronic QE−MNPs coupling.

https://doi.org/10.1021/acs.nanolett.1c03202
Nano Lett. 2021, 21, 8466−8473

In conclusion, we have identified the role played by electronic coupling in the optical response of a canonical hybrid system consisting of a two-level quantum emitter (QE) placed in a nanogap formed by two spherical metal nanoparticles (MNPs). Using a quantum many-body model, we have demonstrated the quenching of the QE exciton originated by the hybridization of the excited states at the QE and the electronic states at the MNPs. This exciton quenching drastically affects the optoelectronic response of the hybrid QE−MNPs system. Furthermore, the depletion of the potential barrier within subnanometric gaps due to the presence of the QE gives rise to a low-energy electron-transfer resonance at $\omega_{CT} \sim 0.1-0.2$ eV, even for situations where the electronic states of the QE do not act as a gateway for electron transport between the MNPs. Our findings are expected to qualitatively apply for plasmon−exciton systems with different electronic structure of the nanoconstituents, since they are based on general and robust quantum-mechanical phenomena such as electron tunneling and electron transfer between the metal and the QE. Thus, the results obtained here stress the need to consider the QE−MNPs electronic coupling, in addition to the standard electromagnetic interaction, in order to unveil fundamental quantum effects related to charge transfer, often affecting the practical implementation of nanoscale sources of photon emission and optoelectronic nanodevices.

■ ASSOCIATED CONTENT

Supporting Information

The Supporting Information is available free of charge at https://pubs.acs.org/doi/10.1021/acs.nanolett.1c03202.

Explanation of the TDDFT model used to describe the QE and the coupled QE−MNPs structure, details on the numerical method adopted to calculate the classical optical response of the QE−MNPs system, analysis of the electronic QE−MNPs coupling in a resonant exciton−plasmon system analysis of the coupling strength to identify the strong-coupling regime in a resonant exciton-plasmon system, comparison of the results obtained with a semiclassical model to further confirm the role of the electronic QE−MNPs coupling, and results of the charge-transfer resonances at low energies for different QEs (PDF)

The dataset corresponding to the results shown in the figures of this paper can be found at: http://hdl.handle.net/10261/249946

■ AUTHOR INFORMATION

Corresponding Authors

Antton Babaze − *Materials Physics Center CSIC-UPV/EHU, 20018 Donostia-San Sebastián, Spain; Donostia International Physics Center DIPC, 20018 Donostia-San Sebastián, Spain;* orcid.org/0000-0002-9775-062X; Email: anttonbabaze@dipc.org

Javier Aizpurua − *Materials Physics Center CSIC-UPV/EHU, 20018 Donostia-San Sebastián, Spain; Donostia International Physics Center DIPC, 20018 Donostia-San Sebastián, Spain;* orcid.org/0000-0002-1444-7589; Email: aizpurua@ehu.eus

Authors

Ruben Esteban − *Materials Physics Center CSIC-UPV/EHU, 20018 Donostia-San Sebastián, Spain; Donostia International Physics Center DIPC, 20018 Donostia-San Sebastián, Spain;* orcid.org/0000-0002-9175-2878

Andrei G. Borisov − *Institut des Sciences Moléculaires d'Orsay, UMR 8214 CNRS-Université Paris-Saclay, Cedex 91405 Orsay, France;* orcid.org/0000-0003-0819-5028

Complete contact information is available at: https://pubs.acs.org/10.1021/acs.nanolett.1c03202

Notes

The authors declare no competing financial interest.

■ ACKNOWLEDGMENTS

A.B. thanks the hospitality and nice atmosphere at the Institut des Sciences Moléculaires d'Orsay, France, and also the Department of Education of the Basque Government for a predoctoral fellowship (PRE2017_1_0267). A.B., R.E., and J.A. acknowledge project PID2019-107432GB-I00 from Spanish MICINN and project PI2017-30 and grant IT1164-19 for consolidated groups of the Basque University system from the Department of Education of the Basque Government. This project has received funding from the European Union's Horizon 2020 research and innovation program under grant agreement no. 861950, project POSEIDON.

■ REFERENCES

(1) Fort, E.; Grésillon, S. Surface enhanced fluorescence. *J. Phys. D: Appl. Phys.* **2008**, *41*, 013001.

(2) Lakowicz, J. R. *Principles of fluorescence spectroscopy*, 3rd ed.; Springer Science & business media: Baltimore, 2013.

(3) Gupta, S. N.; Bitton, O.; Neuman, T.; Esteban, R.; Chuntonov, L.; Aizpurua, J.; Haran, G. Complex plasmon-exciton dynamics revealed through quantum dot light emission in a nanocavity. *Nat. Commun.* **2021**, *12*, 1310.

(4) Doppagne, B.; Neuman, T.; Soria-Martinez, R.; López, L. E. P.; Bulou, H.; Romeo, M.; Berciaud, S.; Scheurer, F.; Aizpurua, J.; Schull, G. Single-molecule tautomerization tracking through space-and time-resolved fluorescence spectroscopy. *Nat. Nanotechnol.* **2020**, *15*, 207−211.

(5) Yang, B.; Chen, G.; Ghafoor, A.; Zhang, Y.; Zhang, Y.; Zhang, Y.; Luo, Y.; Yang, J.; Sandoghdar, V.; Aizpurua, J.; Dong, Z.; Hou, J. G. Sub-nanometre resolution in single-molecule photoluminescence imaging. *Nat. Photonics* **2020**, *14*, 693−699.

(6) Hoang, T. B.; Akselrod, G. M.; Mikkelsen, M. H. Ultrafast room-temperature single photon emission from quantum dots coupled to plasmonic nanocavities. *Nano Lett.* **2016**, *16*, 270−275.

(7) Törmä, P.; Barnes, W. L. Strong coupling between surface plasmon polaritons and emitters: a review. *Rep. Prog. Phys.* **2015**, *78*, 013901.

(8) Melnikau, D.; Esteban, R.; Savateeva, D.; Sánchez-Iglesias, A.; Grzelczak, M.; Schmidt, M. K.; Liz-Marzán, L. M.; Aizpurua, J.; Rakovich, Y. P. Rabi splitting in photoluminescence spectra of hybrid systems of gold nanorods and J-aggregates. *J. Phys. Chem. Lett.* **2016**, *7*, 354−362.

(9) Santhosh, K.; Bitton, O.; Chuntonov, L.; Haran, G. Vacuum Rabi splitting in a plasmonic cavity at the single quantum emitter limit. *Nat. Commun.* **2016**, *7*, 11823.

(10) Chikkaraddy, R.; de Nijs, B.; Benz, F.; Barrow, S. J.; Scherman, O. A.; Rosta, E.; Demetriadou, A.; Fox, P.; Hess, O.; Baumberg, J. J. Single-molecule strong coupling at room temperature in plasmonic nanocavities. *Nature* **2016**, *535*, 127−130.

(11) Baranov, D. G.; Wersäll, M.; Cuadra, J.; Antosiewicz, T. J.; Shegai, T. Novel nanostructures and materials for strong light-matter interactions. *ACS Photonics* **2018**, *5*, 24−42.

(12) Leng, H.; Szychowski, B.; Daniel, M.-C.; Pelton, M. Strong coupling and induced transparency at room temperature with single quantum dots and gap plasmons. *Nat. Commun.* **2018**, *9*, 4012.
(13) Kockum, A. F.; Miranowicz, A.; de Liberato, S.; Savasta, S.; Nori, F. Ultrastrong coupling between light and matter. *Nature Reviews Physics* **2019**, *1*, 19−40.
(14) Ford, G. W.; Weber, W. H. Electromagnetic interactions of molecules with metal surfaces. *Phys. Rep.* **1984**, *113*, 195−287.
(15) Govorov, A. O.; Bryant, G. W.; Zhang, W.; Skeini, T.; Lee, J.; Kotov, N. A.; Slocik, J. M.; Naik, R. R. Exciton-Plasmon Interaction and Hybrid Excitons in Semiconductor-Metal Nanoparticle Assemblies. *Nano Lett.* **2006**, *6*, 984−994.
(16) Carminati, R.; Greffet, J.-J.; Henkel, C.; Vigoureux, J. Radiative and non-radiative decay of a single molecule close to a metallic nanoparticle. *Opt. Commun.* **2006**, *261*, 368−375.
(17) Muskens, O.; Giannini, V.; Sánchez-Gil, J. A.; Gómez Rivas, J. Strong enhancement of the radiative decay rate of emitters by single plasmonic nanoantennas. *Nano Lett.* **2007**, *7*, 2871−2875.
(18) Rogobete, L.; Kaminski, F.; Agio, M.; Sandoghdar, V. Design of plasmonic nanoantennae for enhancing spontaneous emission. *Opt. Lett.* **2007**, *32*, 1623−1625.
(19) Taminiau, T. H.; Stefani, F.; van Hulst, N. F. Single emitters coupled to plasmonic nano-antennas: angular emission and collection efficiency. *New J. Phys.* **2008**, *10*, 105005.
(20) Novotny, L.; van Hulst, N. Antennas for light. *Nat. Photonics* **2011**, *5*, 83−90.
(21) Feibelman, P. J. Surface electromagnetic fields. *Prog. Surf. Sci.* **1982**, *12*, 287−407.
(22) Persson, B. N. J.; Lang, N. D. Electron-hole-pair quenching of excited states near a metal. *Phys. Rev. B: Condens. Matter Mater. Phys.* **1982**, *26*, 5409−5415.
(23) Apell, P.; Ljungbert, Å. A general non-local theory for the electromagnetic response of a small metal particle. *Phys. Scr.* **1982**, *26*, 113.
(24) Tserkezis, C.; Mortensen, N. A.; Wubs, M. How nonlocal damping reduces plasmon-enhanced fluorescence in ultranarrow gaps. *Phys. Rev. B: Condens. Matter Mater. Phys.* **2017**, *96*, 085413.
(25) Tserkezis, C.; Wubs, M.; Mortensen, N. A. Robustness of the Rabi splitting under nonlocal corrections in plexcitonics. *ACS Photonics* **2018**, *5*, 133−142.
(26) Ciracì, C.; Jurga, R.; Khalid, M.; Della Sala, F. Plasmonic quantum effects on single-emitter strong coupling. *Nanophotonics* **2019**, *8*, 1821−1833.
(27) Trügler, A.; Hohenester, U. Strong coupling between a metallic nanoparticle and a single molecule. *Phys. Rev. B: Condens. Matter Mater. Phys.* **2008**, *77*, 115403.
(28) Waks, E.; Sridharan, D. Cavity QED treatment of interactions between a metal nanoparticle and a dipole emitter. *Phys. Rev. A: At., Mol., Opt. Phys.* **2010**, *82*, 043845.
(29) Delga, A.; Feist, J.; Bravo-Abad, J.; Garcia-Vidal, F. Quantum Emitters Near a Metal Nanoparticle: Strong Coupling and Quenching. *Phys. Rev. Lett.* **2014**, *112*, 253601.
(30) Esteban, R.; Aizpurua, J.; Bryant, G. W. Strong coupling of single emitters interacting with phononic infrared antennae. *New J. Phys.* **2014**, *16*, 013052.
(31) Corni, S.; Tomasi, J. Lifetimes of electronic excited states of a molecule close to a metal surface. *J. Chem. Phys.* **2003**, *118*, 6481−6494.
(32) Andreussi, O.; Corni, S.; Mennucci, B.; Tomasi, J. Radiative and nonradiative decay rates of a molecule close to a metal particle of complex shape. *J. Chem. Phys.* **2004**, *121*, 10190−10202.
(33) Galego, J.; Garcia-Vidal, F. J.; Feist, J. Cavity-induced modifications of molecular structure in the strong-coupling regime. *Phys. Rev. X* **2015**, *5*, 041022.
(34) Neuman, T.; Esteban, R.; Casanova, D.; García-Vidal, F.; Aizpurua, J. Coupling of molecular emitters and plasmonic cavities beyond the point-dipole approximation. *Nano Lett.* **2018**, *18*, 2358−2364.
(35) Aguilar-Galindo, F.; Díaz-Tendero, S.; Borisov, A. G. Electronic Structure Effects in the Coupling of a Single Molecule with a Plasmonic Antenna. *J. Phys. Chem. C* **2019**, *123*, 4446−4456.
(36) Avouris, P.; Persson, B. N. J. Excited states at metal surfaces and their non-radiative relaxation. *J. Phys. Chem.* **1984**, *88*, 837−848.
(37) Tully, J. C. Chemical Dynamics at Metal Surfaces. *Annu. Rev. Phys. Chem.* **2000**, *51*, 153−178.
(38) Gebauer, W.; Langner, A.; Schneider, M.; Sokolowski, M.; Umbach, E. Luminescence quenching of ordered π-conjugated molecules near a metal surface: Quaterthiophene and PTCDA on Ag(111). *Phys. Rev. B: Condens. Matter Mater. Phys.* **2004**, *69*, 155431.
(39) Chong, M. C.; Reecht, G.; Bulou, H.; Boeglin, A.; Scheurer, F.; Mathevet, F.; Schull, G. Narrow-Line Single-Molecule Transducer between Electronic Circuits and Surface Plasmons. *Phys. Rev. Lett.* **2016**, *116*, 036802.
(40) Marinica, D.; Lourenço-Martins, H.; Aizpurua, J.; Borisov, A. G. Plexciton quenching by resonant electron transfer from quantum emitter to metallic nanoantenna. *Nano Lett.* **2013**, *13*, 5972−5978.
(41) Song, P.; Nordlander, P.; Gao, S. Quantum mechanical study of the coupling of plasmon excitations to atomic-scale electron transport. *J. Chem. Phys.* **2011**, *134*, 074701.
(42) Song, P.; Meng, S.; Nordlander, P.; Gao, S. Quantum plasmonics: Symmetry-dependent plasmon-molecule coupling and quantized photoconductances. *Phys. Rev. B: Condens. Matter Mater. Phys.* **2012**, *86*, 121410.
(43) Kulkarni, V.; Manjavacas, A. Quantum effects in charge transfer plasmons. *ACS Photonics* **2015**, *2*, 987−992.
(44) Garcia-Gonzalez, P.; Varas, A.; Garcia-Vidal, F.; Rubio, A. Single-atom control of the optoelectronic response in sub-nanometric cavities. 2019, 1903.08443. arXiv. https://arxiv.org/abs/1903.08443 (accessed September 1, 2021).
(45) Rossi, T. P.; Shegai, T.; Erhart, P.; Antosiewicz, T. J. Strong plasmon-molecule coupling at the nanoscale revealed by first-principles modeling. *Nat. Commun.* **2019**, *10*, 3336.
(46) Tan, S. F.; Wu, L.; Yang, J. K.; Bai, P.; Bosman, M.; Nijhuis, C. A. Quantum plasmon resonances controlled by molecular tunnel junctions. *Science* **2014**, *343*, 1496−1499.
(47) Wang, T.; Nijhuis, C. A. Molecular electronic plasmonics. *Applied Materials Today* **2016**, *3*, 73−86.
(48) Du, W.; Wang, T.; Chu, H.-S.; Nijhuis, C. A. Highly efficient on-chip direct electronic-plasmonic transducers. *Nat. Photonics* **2017**, *11*, 623−627.
(49) Parzefall, M.; Szabó, Á.; Taniguchi, T.; Watanabe, K.; Luisier, M.; Novotny, L. Light from van der Waals quantum tunneling devices. *Nat. Commun.* **2019**, *10*, 292.
(50) Fedorov, A.; Krasnov, P.; Visotin, M.; Tomilin, F.; Polyutov, S.; Ågren, H. Charge-transfer plasmons with narrow conductive molecular bridges: A quantum-classical theory. *J. Chem. Phys.* **2019**, *151*, 244125.
(51) Halas, N. J.; Lal, S.; Chang, W.-S.; Link, S.; Nordlander, P. Plasmons in Strongly Coupled Metallic Nanostructures. *Chem. Rev.* **2011**, *111*, 3913−3961.
(52) Savasta, S.; Saija, R.; Ridolfo, A.; di Stefano, O.; Denti, P.; Borghese, F. polaritons: Vacuum Rabi Splitting with a Single Quantum Dot in the Center of a Dimer antenna. *ACS Nano* **2010**, *4*, 6369−6376.
(53) Manjavacas, A.; García de Abajo, F. J.; Nordlander, P. Quantum Plexcitonics: Strongly Interacting Plasmons and Excitons. *Nano Lett.* **2011**, *11*, 2318−2323.
(54) Li, R.-Q.; Hernángomez-Pérez, D.; García-Vidal, F. J.; Fernández-Domínguez, A. I. Transformation Optics Approach to Plasmon-Exciton Strong Coupling in Nanocavities. *Phys. Rev. Lett.* **2016**, *117*, 107401.
(55) Gross, E.; Kohn, W. In *Density Functional Theory of Many-Fermion Systems*; Löwdin, P.-O., Ed.; Advances in Quantum Chemistry; Academic Press, 1990; Vol. *21*; pp 255−291.
(56) Marques, M.; Gross, E. Time-Dependent Density Functional Theory. *Annu. Rev. Phys. Chem.* **2004**, *55*, 427−455.

https://doi.org/10.1021/acs.nanolett.1c03202
Nano Lett. 2021, 21, 8466−8473

(57) Ullrich, C. A. *Time-dependent density-functional theory: concepts and applications*; Oxford University Press: Oxford, 2012.
(58) Jones, R. O. Density functional theory: Its origins, rise to prominence, and future. *Rev. Mod. Phys.* **2015**, *87*, 897−923.
(59) Marinica, D.; Kazansky, A.; Nordlander, P.; Aizpurua, J.; Borisov, A. G. Quantum Plasmonics: Nonlinear Effects in the Field Enhancement of a Plasmonic Nanoparticle Dimer. *Nano Lett.* **2012**, *12*, 1333−1339.
(60) Zhang, P.; Feist, J.; Rubio, A.; García-González, P.; García-Vidal, F. Ab initio nanoplasmonics: The impact of atomic structure. *Phys. Rev. B: Condens. Matter Mater. Phys.* **2014**, *90*, 161407.
(61) Guidez, E. B.; Aikens, C. M. Quantum mechanical origin of the plasmon: from molecular systems to nanoparticles. *Nanoscale* **2014**, *6*, 11512−11527.
(62) Barbry, M.; Koval, P.; Marchesin, F.; Esteban, R.; Borisov, A. G.; Aizpurua, J.; Sánchez-Portal, D. Atomistic near-field nanoplasmonics: reaching atomic-scale resolution in nanooptics. *Nano Lett.* **2015**, *15*, 3410−3419.
(63) Rossi, T. P.; Zugarramurdi, A.; Puska, M. J.; Nieminen, R. M. Quantized evolution of the plasmonic response in a stretched nanorod. *Phys. Rev. Lett.* **2015**, *115*, 236804.
(64) Varas, A.; García-González, P.; Feist, J.; García-Vidal, F.; Rubio, A. Quantum plasmonics: from jellium models to ab initio calculations. *Nanophotonics* **2016**, *5*, 409−426.
(65) Marchesin, F.; Koval, P.; Barbry, M.; Aizpurua, J.; Sanchez-Portal, D. Plasmonic response of metallic nanojunctions driven by single atom motion: quantum transport revealed in optics. *ACS Photonics* **2016**, *3*, 269−277.
(66) Selenius, E.; Malola, S.; Kuisma, M.; Häkkinen, H. Charge Transfer Plasmons in Dimeric Electron Clusters. *J. Phys. Chem. C* **2020**, *124*, 12645−12654.
(67) Perera, T.; Gunapala, S. D.; Stockman, M. I.; Premaratne, M. Plasmonic Properties of Metallic Nanoshells in the Quantum Limit: From Single Particle Excitations to Plasmons. *J. Phys. Chem. C* **2020**, *124*, 27694−27708.
(68) Ekardt, W. Dynamical polarizability of small metal particles: self-consistent spherical jellium background model. *Phys. Rev. Lett.* **1984**, *52*, 1925.
(69) Brack, M. The physics of simple metal clusters: self-consistent jellium model and semiclassical approaches. *Rev. Mod. Phys.* **1993**, *65*, 677.
(70) Zhu, W.; Esteban, R.; Borisov, A. G.; Baumberg, J. J.; Nordlander, P.; Lezec, H. J.; Aizpurua, J.; Crozier, K. B. Quantum mechanical effects in plasmonic structures with subnanometre gaps. *Nat. Commun.* **2016**, *7*, 11495.
(71) Sundaramurthy, A.; Crozier, K.; Kino, G.; Fromm, D.; Schuck, P.; Moerner, W. Field enhancement and gap-dependent resonance in a system of two opposing tip-to-tip Au nanotriangles. *Phys. Rev. B: Condens. Matter Mater. Phys.* **2005**, *72*, 165409.
(72) Teperik, T. V.; Nordlander, P.; Aizpurua, J.; Borisov, A. G. Robust subnanometric plasmon ruler by rescaling of the nonlocal optical response. *Phys. Rev. Lett.* **2013**, *110*, 263901.
(73) van Vlack, C.; Kristensen, P. T.; Hughes, S. Spontaneous emission spectra and quantum light-matter interactions from a strongly coupled quantum dot metal-nanoparticle system. *Phys. Rev. B: Condens. Matter Mater. Phys.* **2012**, *85*, 075303.
(74) Babaze, A.; Esteban, R.; Aizpurua, J.; Borisov, A. G. Second-Harmonic Generation from a Quantum Emitter Coupled to a Metallic Nanoantenna. *ACS Photonics* **2020**, *7*, 701−713.
(75) Gonçalves, P.; Christensen, T.; Rivera, N.; Jauho, A.-P.; Mortensen, N. A.; Soljačić, M. Plasmon-emitter interactions at the nanoscale. *Nat. Commun.* **2020**, *11*, 1−13.
(76) Chulkov, E.; Borisov, A.; Gauyacq, J.; Sánchez-Portal, D.; Silkin, V.; Zhukov, V.; Echenique, P. Electronic excitations in metals and at metal surfaces. *Chem. Rev.* **2006**, *106*, 4160−4206.
(77) Esteban, R.; Borisov, A. G.; Nordlander, P.; Aizpurua, J. Bridging quantum and classical plasmonics with a quantum-corrected model. *Nat. Commun.* **2012**, *3*, 1−9.
(78) Duan, H.; Fernández-Domínguez, A. I.; Bosman, M.; Maier, S. A.; Yang, J. K. Nanoplasmonics: classical down to the nanometer scale. *Nano Lett.* **2012**, *12*, 1683−1689.
(79) Savage, K. J.; Hawkeye, M. M.; Esteban, R.; Borisov, A. G.; Aizpurua, J.; Baumberg, J. J. Revealing the quantum regime in tunnelling plasmonics. *Nature* **2012**, *491*, 574−577.
(80) Scholl, J. A.; García-Etxarri, A.; Koh, A. L.; Dionne, J. A. Observation of Quantum Tunneling between Two Plasmonic Nanoparticles. *Nano Lett.* **2013**, *13*, 564−569.
(81) Wu, L.; Duan, H.; Bai, P.; Bosman, M.; Yang, J. K.; Li, E. Fowler-Nordheim tunneling induced charge transfer plasmons between nearly touching nanoparticles. *ACS Nano* **2013**, *7*, 707−716.
(82) Esteban, R.; Zugarramurdi, A.; Zhang, P.; Nordlander, P.; García-Vidal, F. J.; Borisov, A. G.; Aizpurua, J. A classical treatment of optical tunneling in plasmonic gaps: extending the quantum corrected model to practical situations. *Faraday Discuss.* **2015**, *178*, 151−183.
(83) Aguirregabiria, G.; Marinica, D. C.; Esteban, R.; Kazansky, A. K.; Aizpurua, J.; Borisov, A. G. Role of electron tunneling in the nonlinear response of plasmonic nanogaps. *Phys. Rev. B: Condens. Matter Mater. Phys.* **2018**, *97*, 115430.
(84) Bitton, O.; Gupta, S. N.; Haran, G. Quantum dot plasmonics: from weak to strong coupling. *Nanophotonics* **2019**, *8*, 559−575.

https://doi.org/10.1021/acs.nanolett.1c03202
Nano Lett. 2021, 21, 8466−8473